Earthquake recurrence-time variations with and without fault-zone interactions

Thorsten W. Becker* and Harro Schmeling

Institut für Meteorologie und Geophysik, J. W. Goethe-Universität Frankfurt am Main, Feldbergstraße 47, D-60323, Frankfurt am Main, Germany

SUMMARY

The macroscopic behaviour of a fault zone can be described by a classic Coulomb friction law and static–kinetic rheology. The critical failure stress leading to the activation of a single shear zone segment then depends on the normal stress acting on the future fault plane. It is known that the seismic cycle on a main fault patch can be modulated by surrounding fault activations, leading to interaction with the main segment, or by other external stress perturbations.

The results presented here stem from analytical assessments and 2-D numerical elastic models. They show that an earthquake recurrence-time variation with continuing deformation system development is not necessarily connected to fault interaction processes under the above assumptions. Instead, aperiodicity can result from a non-ideal orientation of the rupture plane in the simplest possible homogeneous stress field, even when constant loading rate and frictional parameters are assumed. This effect can still be found in the multifault geometries we studied, where the interaction of segments determines the seismicity patterns of the system to varying extents.

Our results suggest that a stable earthquake periodicity on non-changing fault sets will seldom be found in nature. We propose a reconsideration of the ideas leading to a hypothesized steady seismic cycle in earthquake prediction models.

Key words: earthquake prediction, fault models, transform faults.

1 INTRODUCTION

The elastic rebound model of Reid (1910) has been applied to interplate earthquakes occurring at shear zones. Plate tectonic displacement rates are usually assumed to be constant, leading to a cyclic failure of rocks on faults within the shear zone. With the additional constraint of a constant failure stress and a complete stress drop, Reid's model predicts a periodic seismic cycle at single, isolated shear-zone patches. Recognizing that stresses are usually not completely released, more advanced descriptive models have been proposed (e.g. Shimazaki & Nakata 1980; for a review see Scholz 1990, Chapter 5). These 'time- or slip-predictable' models incorporate varying stress drops but do not offer a mechanism determining how and why the stress drop may vary in detail. Recently, Mulargia & Gasperini (1995) examined the applicability of both models to seismicity in Italy and re-examined the work of other authors for different regions; they found that neither model matches the data well.

Evidence in favour of or against the basic concept of regular patterns in seismicity is contradictory and sparse. One well-known small-scale example of a transform fault segment showing almost exact periodicity over historical times is the Parkfield, California, series examined by Bakun & McEvilly (1984) and shown in Fig. 1. The palaeoseismic approach allows the significant extension of the sampling period of the seismicity data sets (e.g. Sieh, Stuiver & Brillinger 1989; Calpin 1996), but results are only available for a few shear-zone segments today, or are of limited accuracy. In addition, palaeoseismic studies are mainly restricted to earthquakes that ruptured the surface. One of the few examples of a non-historical and accurate record of seismicity that was derived with palaeoseismic methods is the Pallett Creek, California, sequence shown in Fig. 2. The data show the intermittence of quiescent 'kinks' in three fairly periodic sequences that are discussed by Sieh *et al.* (1989).

Nishenko & Buland (1987) and Goes (1996) conducted a global survey of large earthquake recurrence intervals from historical and palaeoseismic data catalogues. Both concluded that the recurrence times of the earthquakes were distributed around average values following probabilistic distributions and hence were only quasi-periodic, although Goes found larger irregularities.

* Now at: Harvard University, Department of Earth and Planetary Sciences, 20 Oxford St, Cambridge, MA 02138, USA. E-mail: becker@eps.harvard.edu
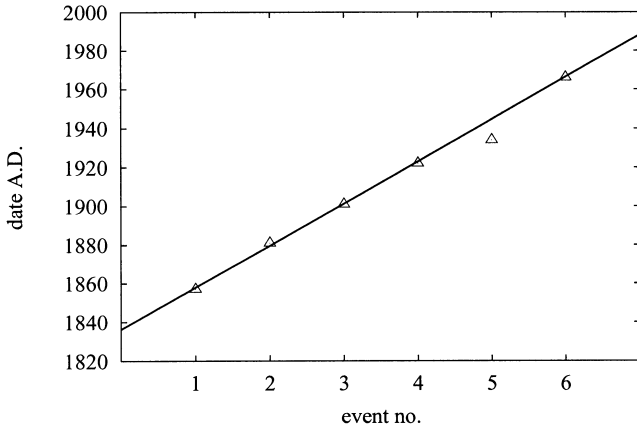
Figure 1. Earthquake series at Parkfield, California; data from Bakun & McEvilly (1984). The linear fit shown neglects event no. 5. (Note that the seventh event, which could have been expected, is overdue.)

These results and other findings have led several authors in the last few years to highlight the importance of fault interactions on the basis of physical models (e.g. Rundle 1988a; Palmer *et al.* 1995; Ruff 1996) while others have emphasized the irregular and unpredictable aspects of seismicity (e.g. Chen, Bak & Obukhov 1991).

Given the observations of both regular and varying recurrence times, our aim is to use physical models to determine some of the parameters that control recurrence times. Using simple analytic estimations and numerical finite-element (FE) models, we show that stable earthquake recurrence cycles are to be expected only as an outcome of very special configurations, even in the case of a single fault. Our results suggest that assumptions behind the time-predictable earthquake recurrence model, such as a constant loading rate, should be reconsidered, even when no time dependence of frictional parameters is invoked.

Our models are 2-D and behave purely elastically except at 'faults' or 'cracks', where slip is allowed following a static–kinetic friction law. Furthermore, we use simplified geometries only coarsely resembling real fault zones. They are therefore more elementary approaches than those of other authors, who have incorporated more complicated rheological constitutive laws and viscous layers into single-fault models (e.g. Li &
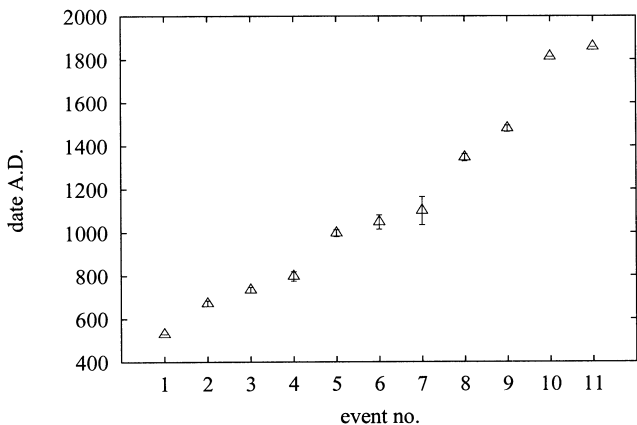
Figure 2. Earthquake series at Pallett Creek, California; data from Sieh *et al.* (1989).

Rice 1987; Bonafede, Dragoni & Morelli 1986; Lyzenga, Raefsky & Mulligan 1991), or more complex geometries (e.g. Stuart 1986; Rundle 1988b; Ward 1996; Deng & Sykes 1997). However, based on mechanically consistent calculations, our simplified approach allows us to extract relations between fault orientation, fault interaction and earthquake sequences in our model that we consider to be of general importance. This study should thus serve to shed some light on the nature of the physical processes that determine shear zone seismicity.

2 THEORETICAL APPROACH

2.1 The Coulomb failure criterion revisited

We are interested in the macroscopic properties of shear zones and only deal with strike-slip faults located in the upper lithosphere. Brittle–elastic behaviour can be considered the predominant rheology there (Segall & Pollard 1980). We assume negligible variations of the deformation field with depth (large fault-plane depth extent) and choose a plane-strain approximation. To first order, the brittle failure of rock can then be described by the Navier–Coulomb criterion for intact material, which in its functional dependence is nothing more than Amonton's friction law. For pre-existing fault planes, the laboratory data for the shear stress needed to initiate rupture can be fitted with one set of parameters for different rock types (Byerlee 1978). This relationship is sometimes called Byerlee's law:

$$\tau_c(\beta) = \mu_s \sigma_n(\beta) \,, \tag{1}$$

where τ_c denotes the critical shear stress, σ_n is the normal stress acting on the fault plane and μ_s is the coefficient of static friction. The pore pressure and cohesive force found in the common notation have been set to zero for simplicity. β indicates the fault orientation with respect to the first principal stress axis, σ_1, on the σ_1–σ_3 plane, and σ_2 has been assumed vertical (*cf*. Fig. 3; following rock mechanics convention, compressive stresses are taken as positive). In general,

$$\sigma_n(\beta) = \bar{\sigma}_n - \tau_{max} \cos(2\beta) \tag{2}$$

and

$$\tau(\beta) = \tau_{max} \sin(2\beta) \tag{3}$$

hold, where the maximum shear stress and the mean horizontal stress are defined by $\tau_{max} := (\sigma_1 - \sigma_3)/2$ and $\bar{\sigma}_n := (\sigma_1 + \sigma_3)/2$, respectively. Following Stein & Lisowski (1983), the status of rock obeying the failure criterion (1) can be measured by the 'Coulomb stress', σ_c, defined by

$$\sigma_c(\beta) := |\tau(\beta)| - \mu_s \sigma_n(\beta) = C(\beta)\tau_{max} - \mu_s \bar{\sigma}_n \,. \tag{4}$$

Allowing for left- and right-lateral slip, only absolute values of τ are treated. The factor $C(\beta)$ is given by

$$C(\beta) := |\sin(2\beta)| + \mu_s \cos(2\beta) \,. \tag{5}$$

If σ_c reaches zero or becomes positive for a particular fault orientation, the empirical law predicts rupture initiation. It is often assumed that all possible fault-plane orientations exist in a strongly fractured crust. Thus, eq. (1) can be rewritten in terms of the principal stresses:

$$\sigma_1 = a\sigma_3 \,, \quad \text{where} \quad a := \frac{\sqrt{1+\mu_s^2} + \mu_s}{\sqrt{1+\mu_s^2} - \mu_s} \,, \tag{6}$$

which holds for the fault orientations with $\sigma_c(\beta) = 0$. These angles can be calculated by

$$\beta_{\max} = \left(n + \frac{1}{2}\right)\pi \pm \left(\frac{\arctan(\mu_s)}{2} + \frac{\pi}{4}\right), \quad n = 0, \pm 1 \dots . \quad (7)$$

The formalism based on the calculation of σ_c appears to be an indicator for the *in situ* status of faults (e.g. Stein & Lisowski 1983; Harris, Simpson & Reasenberg 1995; King, Stein & Lin 1994). We adapt this method to model the static ('instantaneous') elastic fault interactions and disregard other, possibly time-dependent, interaction processes, for example those due to viscoelastic stress diffusion (e.g. Scholz 1974; Bonafede *et al.* 1986; Heimpel & Olson 1996).

2.2 Static–kinetic friction laws and dynamical aspects

Earthquake rupture in our models is achieved by using the Coulomb criterion as described in the previous section and a 'static–kinetic' friction law. The latter mimics stick-slip earthquake rupture series by the introduction of a second frictional parameter μ_d and will be described later. We do not regard any changes of the frictional parameters with time and do not include proper dynamical effects.

These assumptions may be justified as follows. There are basically two possibilities as to why the static coefficient of friction might vary with time (and not only due to heterogeneities in the medium) and thus influence the seismic cycle. One possibility is the presence of pore fluids, where the effect of increased pore pressure is to reduce the effective normal stress. For undrained rock and hydrostatic conditions, this can be rephrased as a modified $\mu'_s := (1 - B)\mu_s$, where B is a Skempton coefficient. The time-dependent variation of pore pressure has been proposed as being responsible for the delayed triggering of earthquakes (e.g. Nur & Booker 1972; Hudnut, Seeber & Pacheco 1989). The importance of this effect is unclear at the moment, and we will not take it into account any further.

The second effect that leads to varying values of μ_s is described by 'rate- and state-dependent' friction (for a recent review see Marone 1998). These laboratory-derived, semi-empirical friction laws predict variations of the coefficient of friction as a function of the slip velocity at the rupture time itself (velocity weakening or strengthening) and as a consequence of the loading history of a rock surface (loading rate and 'healing time' before rupture). Given the observation that laboratory measurements of friction cannot be explained by a law as simple as eq. (1) with a constant μ_s, there is still some ambiguity about the general validity of the fitting parameters obtained for various experimental conditions and rock samples. For instance, it is not clear which micromechanical mechanism accounts for the transition from velocity weakening to velocity strengthening that is observed in some experiments for different loading rates. A particular problem in the application of laboratory-derived laws to large-scale phenomena such as earthquakes in the lithosphere (e.g. Marone, Vidale & Ellsworth 1995) is that it is not known how the physical mechanisms and the relevant parameters such as the critical slip length scale. This is emphasized by the work of Schmittbuhl, Vilotte & Roux (1996). Using a numerical renormalization approach, the authors found that a small-scale velocity-weakening friction law is transformed into an apparent classical Coulomb friction law with well-defined static and kinetic friction values on a larger scale.

The quasi-dynamic static–kinetic rupture model we use mimics the dynamic overshoot effect that arises from the accelerated rock masses after the static friction has been overcome. Neglecting dissipative effects and seismic wave radiation, the law describes the shear stress decrease on the rupture plane. Hence, τ will not drop from τ_c to the value prescribed by the friction law via $\tau_k = \sigma_n\mu_k$ (where μ_k is the kinetic friction coefficient), but to a lower value obtained from the product of σ_n and a new parameter, μ_d. When a constant σ_n and an overshoot shear stress reduction by the same amount as given by $\tau_c - \tau_k$ is assumed, the 'dynamic' friction parameter can be estimated by $\mu_d = 2\mu_k - \mu_s$ (e.g. Rice & Tse 1986). The dynamic overshoot effect that is prescribed here *a priori* can also be observed in dynamical calculations based on the classical friction law, such as that of Burridge & Halliday (1971).

Rice & Tse (1986) present numerical calculations for stick-slip cycles, where they investigate various rate- and state-dependent friction laws. For a reasonable range of parameters, these laws still exhibit a rupture behaviour that roughly resembles that of the quasi-dynamic models, if rupture initiation and propagation effects are neglected. In addition to the reasons stated above, and because the influence of these effects is not the issue of our examination, we use the static–kinetic scheme and do not incorporate other friction laws at this time.

Furthermore, faults in our models are not allowed to grow but are restricted to their initial length. This leads to unreasonably high stress accumulations at the crack tips over many earthquake cycles. They can be interpreted to first order in the linear fracture mechanic's small-scale yielding approach as a virtual fault growing by a small amount. However, a fully consistent approach should take the finite strength of the material into account. This is a different problem to that approached by us, and more elaborate studies have addressed it, such as that of Bonafede, Dragoni & Boschi (1985).

2.3 Varying stress drop and seismic cycles

When a rupture at a point $\mathbf{x}$ is initiated at a time t_1 and terminated at a time t_2, the static–kinetic stress drop can be calculated following the assumptions explained above by

$$\Delta\sigma(\mathbf{x}, t_1, t_2) = \mu_s(\mathbf{x})\sigma_n(\mathbf{x}, t_1) - \mu_d(\mathbf{x})\sigma_n(\mathbf{x}, t_2). \quad (8)$$

If σ_n remains constant during the rupture $[\sigma_n(t_1) = \sigma_n(t_2) = \sigma_n(t)]$, the average value along the fault is simply given by $\Delta\sigma(t) = (\mu_s - \mu_d)\sigma_n(t) = \Delta\mu\sigma_n(t)$. This equation is valid for an isolated fault in a homogeneous stress field, but may be altered when other faults—rupturing at the same time—interfere. In the simplest case, we may expect that the failure of a fault segment occurs when the reduced stress is re-established by constantly increasing background deformation. This process would result in a seismic period T_s for earthquakes rupturing the whole fault, which can be estimated by

$$T_s(t) = \frac{\Delta\mu\sigma_n(t)}{\dot{\sigma}_c}. \quad (9)$$

Here $\dot{\sigma}_c$ denotes the rate of Coulomb stress increase and t is the time of the previous stress drop. As discussed in Section 2.2, we assume that it is justified to average $\Delta\mu$ along the fault and neglect any possible time dependence of the static or dynamic friction coefficient.

In the following models a progressive homogeneous simple-shear deformation is added to a depth-averaged background stress p_b acting on the shear zone (Fig. 3). This set-up is supposed to represent a transform plate boundary setting. The corresponding large-scale background strain rate, $\dot{\gamma}_{xy}$, is calculated by

$$\dot{\gamma}_{xy} = \frac{\Delta w}{l \Delta t}, \quad \text{so that} \quad \tau_{max}(t) = G\dot{\gamma}_{xy}t, \tag{10}$$

where (choosing displacement boundary conditions) Δw is the displacement increment at the boundary of the region of extent l at time step Δt and G denotes the shear modulus connecting shear stress τ to engineering strain γ_{xy} (Fig. 3). The seismic period for a single fault in this homogeneous field can be determined by combining eqs (2) and (9) and setting $\bar{\sigma}_n = p_b$:

$$T_s(t) = \frac{\Delta\mu p_b}{G\dot{\gamma}_{xy}C(\beta)} - \frac{\Delta\mu \cos(2\beta)}{C(\beta)}t = T_s^c + \Delta\dot{T}_s t, \tag{11}$$

where T_s^c and $\Delta\dot{T}_s$ have been introduced for brevity. [The singularities of the T_s^c and $\Delta\dot{T}_s$ terms for $C(\beta)=0$ and $C(\beta)<0$ indicate the special situation of no events happening at all. Therefore, eq. (11) is only valid for $|\beta| < (\pi - \arctan(\mu_s))/2$.] The influence of σ_n acting on the fault as a result of the shear deformation vanishes in eq. (2)—and thus also in eq. (11)—for $\beta=45°$. The resulting stress drop is then constant in time and leads to $T_s^c = \Delta\mu p_b/(G\dot{\gamma}_{xy})$. If we assume that $\dot{\gamma}_{xy}$, β and σ_n remain at steady values during a sequence of events, $\Delta\sigma$ and therefore the earthquake magnitude and individual recurrence time would also be expected to remain constant.

Assuming $\beta\neq45°$ and progressive shear deformation, the seismic cycle will not be perfectly periodic, but will show a steady increase or decrease of the time span between events due to the variation of σ_n. When the first event of a sequence happens at T_0, the time the nth earthquake takes place can be estimated by

$$T_n = T_0(1+\Delta\dot{T}_s)^n + T_s^c \frac{(1+\Delta\dot{T}_s)^n - 1}{\Delta\dot{T}_s}. \tag{12}$$

The question arises whether β remains constant for a repeatedly activated fault. The 2-D in-plane crack problem can be solved analytically (e.g. Pollard & Segall 1987). It is possible to calculate the rotation angle Γ for a crack with an initial orientation $\beta=45°$ using the formulae for the maximum displacements u_x^{max} and u_y^{max}. Then, $\Gamma \approx (1-2v)\Delta\sigma/(2G)$ for plane strain and $u_y^{max} \ll a$, where a is the half-crack length and v is Poisson's ratio. The crack will therefore be rotated into the direction of the compressive principal axis by an angle of the order $O(10^{-3})$ degrees for realistic lithospheric parameters such as $v=0.25$, $G=20$ GPa and $\Delta\sigma=1$ MPa. The variation of σ_n associated with this crack rotation can therefore be neglected for single events, whereas this effect may become relevant for cumulative effects. We note that dislocation models for strike-slip on finite rectangular faults in a homogeneous half-space (e.g. Chinnery 1963; Okada 1992) predict no change in normal stress when the fault plane is vertical. Normal stress changes can occur in these models if the fault plane is not vertical or if the slip vector has a dip component.

Under the assumption that $\Delta\mu$ is constant, the $\beta=45°$ configuration can be identified as the only orientation in the simple 2-D shear environment that we have examined that leads to a temporally stable seismic cycle. The predicted variations of recurrence times (*cf*. eq. 11) for isolated faults inclined at $\beta\neq45°$ due to normal stress changes will be compared with models for multifault systems, where eq. (11) no longer holds (Section 4).

3 METHOD

3.1 Numerical approach

We used a standard 2-D FE method as described by Zienkiewicz (1977) and implemented the split-node method introduced by Melosh & Raefsky (1981) to solve the static force equilibrium equation of an elastic medium containing cracks. This method is a load vector manipulation extending the basic FE principle, which is based on minimizing the deformation energy. Split nodes allow for the introduction of dislocations with arbitrary relative displacement vectors (see also Dahm & Becker 1998).

Only cracks of fixed length were considered in all the models presented here. Relative movement of the dislocational elements was restricted to strike-slip, and dislocations (or faults) were represented by chains of split nodes. The relative movement of a split node was initiated during a shear experiment once the local Coulomb stress based on the static friction had risen to a non-negative value. An incremental displacement was estimated and applied, and the differential equations were solved again with the modified load vector. After screening all other split nodes simultaneously for triggered activations, this process was repeated until all active nodes showed shear stresses lower than $\mu_d\sigma_n$. This resulted in a dislocational movement, which we will term 'earthquake', typically consisting of all nodes along the fault. Inhomogeneous stress regimes sometimes lead to irregular activation patterns as multifault systems evolve towards more complex deformation states.
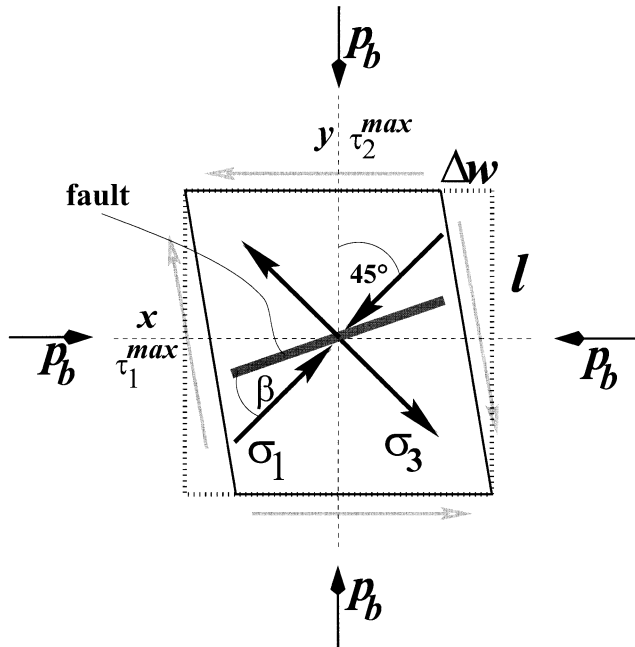
Figure 3. Stress state of simple shear. Axes of τ_{max} correspond to x- and y-axes.

The numerical scheme has been verified by comparison with analytical solutions for a stress-free crack. These formulae contain singularities at the crack tips. An accuracy assessment showed that accurate slip distributions of the corresponding FE model could, however, be achieved with moderate numerical expense. Typical one-crack FE meshes consisted of 5000 elements and had a split-node spacing of $\Delta x \approx 0.02a$ along the fault. We chose triangular elements and linear form functions for numerical efficiency. The mesh was irregularly gridded using a triangulation routine of Shewchuk (1996) under special quality constraints on the minimum inner angle ($32°$) and maximum area $[\approx (a/4)^2]$ of elements to avoid numerical anisotropy and inaccuracy. Typical deviations from the analytical slip solution were of the order of 1 per cent of the mean analytical values, where the resolved shear stress maxima were of the order of five times the stress drop (for details see Becker 1997).

3.2 Model parameters

Besides the geometry of the fault populations examined, the model behaviour depends on the choice of parameters that are thought to describe the material behaviour in nature. Their influence on the seismicity can be evaluated using expressions such as eq. (9), and could be fine-tuned to mimic special tectonic settings, observed earthquake cycles and source parameters. We use the values $p_b = 10$ MPa, $G = 20$ GPa, $\mu_s = 0.6$ and $\mu_d = 0.5$. A single fault aligned along the axis of maximum shear stress ($\beta = 45°$) will then generate earthquakes with an initial stress drop of $\Delta\sigma = 1$ MPa. This $\Delta\sigma$-value can be considered characteristic of large strike-slip earthquakes (e.g. Sykes & Quittmeyer 1981), even though there is much scatter and uncertainty in the independent determination of stress-drop values. Our choice of parameters for μ is somewhat arbitrary, since the field does not provide direct confirmation as to what appropriate values for μ_s and μ_d might be. While rock fracture experiments suggest $\mu_s = 0.85$ for $p_b < 200$ MPa (Byerlee 1978), and rate- and state-dependent friction experiments typically yield values for μ between 0.5 and 0.6 (Marone 1998), the value for fault zones in nature remains unclear for various reasons. The studies of e.g. Lachenbruch & Sass (1980), Reasenberg & Simpson (1992) and Harris *et al.* (1995) suggest a low value for μ_s. Which value of the lithospheric background stress p_b should be used for earthquake rupture calculations is also subject to ongoing debate. However, we are not interested in determining the exact parameters, but in choosing plausible values to predict seismicity in a consistent way under the assumption of the validity of our static–kinetic rupture model approach.

If we assume that a rectangular area around a fault at a plate boundary with extent $a \lessapprox l \lessapprox 2a$ is characteristic of the accumulation of deformation energy due to plates moving with a relative velocity of $v \approx 1.6$ nm s^{-1} (e.g. DeMets *et al.* 1990), the resulting strain rate is 1.6×10^{-14} s$^{-1} \lessapprox \dot\gamma_{xy} \lessapprox 3.2 \times 10^{-14}$ s^{-1} for $2a \approx 100$ km. Taking 3.2×10^{-14} s^{-1} for $\dot\gamma_{xy}$ results in an initial recurrence time of $T_s \approx 50$ yr (*cf*. eq. 11), where a fault of 100 km length is at the upper limit of typical data for earthquakes of magnitude $M_s \approx 7$. All inelastic deformation takes place seismically in our models. If aseismic creep is important for parts of the deformation process at a special fault zone, $\dot\gamma_{xy}$ has to be adjusted accordingly.

The seismic moment, M_0, corresponding to the numerical earthquakes was calculated by averaging the measured slip distribution and multiplying it with a constant depth extent of $W = 15$ km. Magnitudes were assigned using the empirical relation of Purcaru & Berckhemer (1978):

$$\log M_0 = 1.5 M_s + 9.1 \quad [M_0 \text{ in Nm}]. \tag{13}$$

4 RESULTS

4.1 Single-fault geometries

We have numerically examined the behaviour of single faults of various orientations with respect to the homogeneous simple-shear stress field and compared them to the analytic predictions. Two examples with $\beta = 45°$ and $\beta = 29.5°$ will be presented in detail. In the first case, the fault was oriented along the axis of maximum shear stress. The second model corresponds to one of the optimum orientations according to eq. (7). Faults were centred in a computational domain of $400a^2$ to minimize the influence of the boundaries.

Fig. 4 shows the seismicity of the fault oriented such that $\beta = 45°$, where the time needed to reach critical stresses has been skipped. The fault-averaged σ_c-values (Fig. 4a) for each time step and the seismic moment (Fig. 4b) are displayed.

This model showed the expected and roughly regular stick-slip pattern with a sequence of earthquakes whose time-averaged event parameters were $\overline{M_0} \approx 9 \times 10^{19}$ Nm and $\overline{M_s} \approx 7.2$. The constant recurrence time and stress drop can be explained by the finding that each event leads to a normal stress modification that amounts to zero on the fault itself. Hence, $\Delta \dot{T}_s \approx 0$ and the seismic period is $T_s \approx 50$ yr during the whole run. Owing to numerical effects arising from the iteration process, the model produces small trade-offs in τ and σ_n along the fault. They result from the fact that our iteration algorithm solves for a specified stress drop in σ_c, being a function of both shear and normal stresses, and not for τ and σ_n separately, because they may both change due to interaction effects during the earthquake. The resulting fluctuations of τ and σ_n account for only 1 per cent of the mean values. They do, nevertheless, lead to some irregularity and a slight decrease of the seismic moment with time.
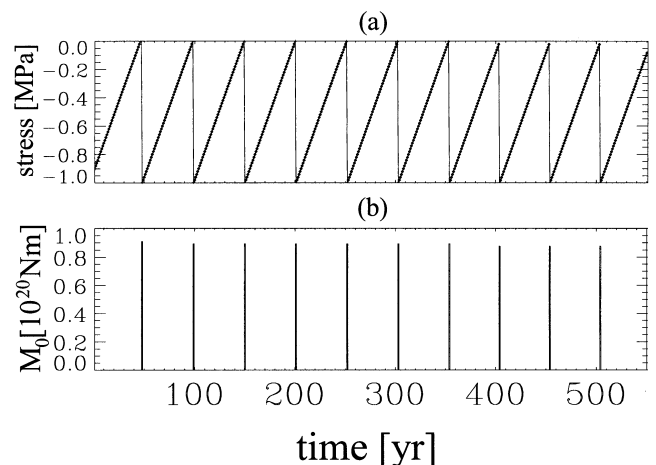
Figure 4. Mean Coulomb stress (σ_c) (a) and seismic moment M_0 (b) for faults oriented such that $\beta = 45°$.

In contrast, the optimally oriented fault exhibited a different behaviour (Fig. 5). Starting with the first earthquake, which occurred earlier than the initial event of the τ_{max}-oriented fault, all subsequent activations showed a reduced seismic moment. They occurred more frequently while the recurrence time decreased steadily. This is a direct consequence of the lowered additional normal stress (*cf*. Fig. 3 and eq. 11), resulting in a decrease of $\Delta\sigma$ with time (Fig. 5a). A closer look at $\langle\sigma_c\rangle$ reveals that these values do not rise exactly to zero for later times. This is again correlated with fluctuations along the rupture plane leading to local σ_c peaks triggering the failure of the whole fault, even though the mean value would not suggest so. If we compare the cumulative values for the mean slip $\Sigma_{t=0}^{550\,yr}\Delta\bar{u}$ or the cumulative seismic moment $\Sigma_{t=0}^{550\,yr}M_0$ with the $\beta=45°$ geometry, the optimally oriented fault turns out to be about 26 per cent more effective in releasing deformation energy. We note that the term 'optimal' has to be viewed in the framework of our model assumptions. That is, all weakness planes are assumed to be realized in the pristine medium. After the optimal plane is then found, its geometry is prescribed *a priori* and will be independent of the stress orientation thereafter.

Fig. 6 compares the theoretical and numerical results for single-fault geometries with four different orientations of β. The seismic cycles for constant T_s ($\beta=45°$) and optimal orientation ($\beta=29.5°$) discussed above are shown. The additional fault ($\beta=60.5°$) is rotated into the compressive deformation field by the same amount as the optimally oriented crack is rotated into the extensive field, whilst the $\beta=54.6°$ model corresponds to the same value of $\Delta\dot{T}_s$, but has a sign opposite to the $\beta=29.5°$ fault. There is no significant deviation between the numerical and analytical results, which indicates that our algorithm is sufficiently stable, and the simplifying assumptions of the analytical derivation are justified for the single-fault problem.

All three seismic cycles with $\beta\neq45°$ diverge from their initial recurrence intervals. Taking the case of $\beta=60.5°$ as an example, the last event of the sequence is accompanied by a preceding quiet period that is 83 per cent longer than that separating the initial earthquakes of the series. This is a substantial modification of the seismic cycle. Furthermore, the two initial earthquakes are the only ones that occur before
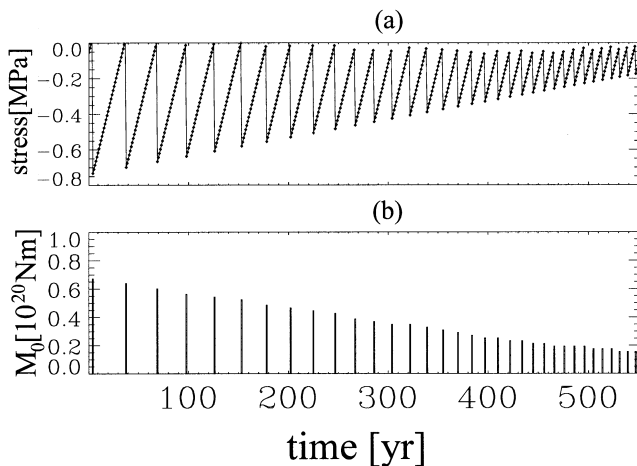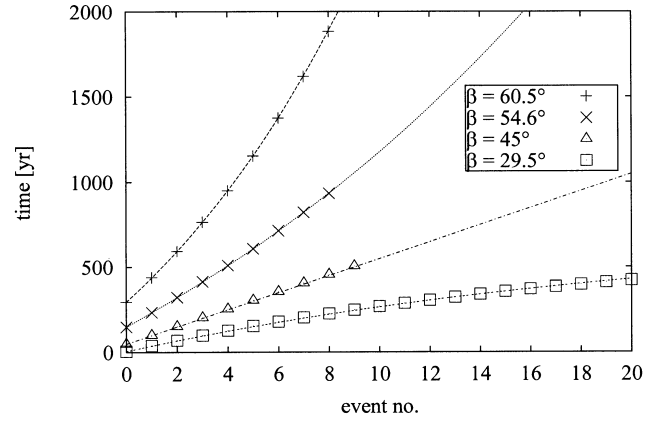
Figure 6. Earthquake sequences of single-fault models for different values of β; lines correspond to eq. (11).

$t=550$ yr, the time span plotted for the first two models discussed. Even though the first earthquakes of the fault are each accompanied by a displacement 40 per cent greater than that of the $\beta=45°$ fault, the total seismic moment released, $\Sigma_{t=0}^{550\,yr}M_0$, is only about one-third of the corresponding value for the $\beta=45°$ fault.

4.2 Interacting faults

4.2.1 Short leftstep and rightstep geometries

We now deal with a simple extension towards more realistic settings, i.e. the configurations shown in Fig. 7. We call them short left- and rightstep geometries after Segall & Pollard (1980).

Both models consist of three fault segments of equal length ($a=50$ km) and were examined as non-intersecting representations of basic fault-zone elements. (They transform into each other if the applied boundary condition is reversed.) Our intention in choosing those geometries is that more complex *en echelon*-style fault systems, as found in nature, can be thought of as being assembled from similar elements.

Models A and B consist of one fault segment with a $\beta=45°$ orientation and two parallel side-faults, which are aligned with $\beta\neq45°$. To examine the effect of the Coulomb stress modification acting on a fault segment due to the neighbouring segments, i.e. the mode of interaction, the explicit Coulomb stress field has to be calculated for the orientation of interest. We found that model A's nos 2 and 3 faults lie in areas of increased proximity to failure when the main fault (no. 1) is activated. This is because the auxiliary faults are subjected to higher shear stress and reduced normal stress. (The normal stress pattern of a mode II crack has characteristic dipolar quadrants; see e.g. Pollard & Segall 1987.) Since model B's auxiliary faults undergo a shear stress increase as well, they also have a higher value of the Coulomb stress criterion after the activation of the main fault. However, σ_c changes by a much smaller amount because the normal stress is increased at the same time for the fault orientation in the stress field. For a suitable orientation of faults and friction values when the fault segments lie completely within a 'stress shadow', the Coulomb stress would even decrease after a main fault rupture.

Fig. 8 shows the seismicity of both models. As their orientations in the homogeneous shear stress field may have

Figure 5. Mean Coulomb stress (σ_c) (a) and seismic moment M_0 (b) for faults oriented such that $\beta=29.5°$.

© 1998 RAS, *GJI* **135**, 165–176
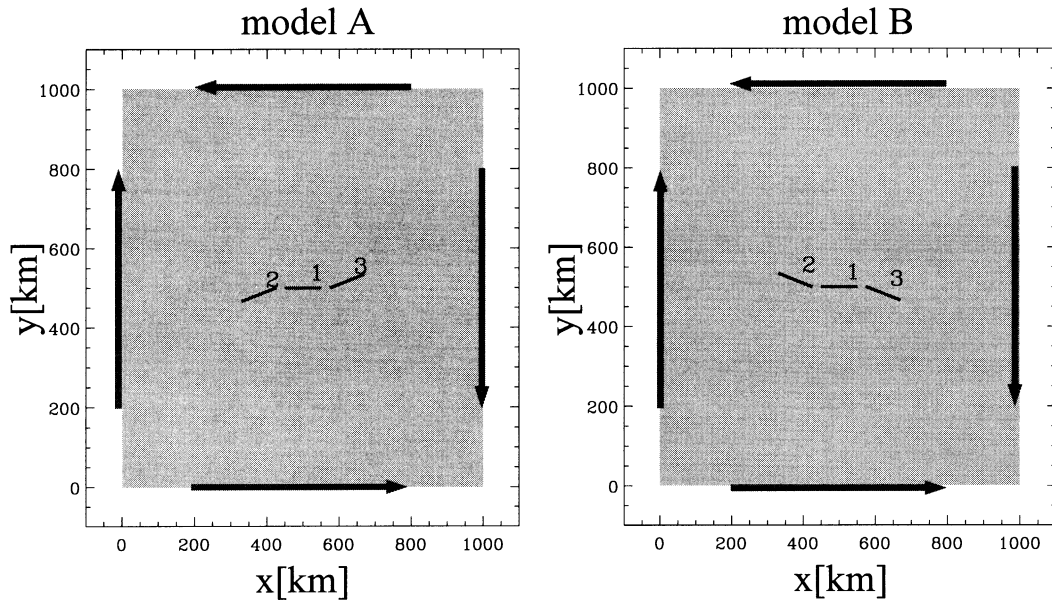
Figure 7. Short leftstep (model A) and rightstep (model B) geometries.

lead us to predict, the leftstep auxiliary faults showed a much more frequent activation than the rightstep faults. The temporal activation patterns of both models consisted of events rupturing the whole shear zone and smaller intermittent earthquakes associated with simultaneous activations of the auxiliary faults alone. A closer inspection reveals the interaction effects leading to a modulation of the undisturbed single-fault cycles. In case A, the recurrence time of earthquakes on fault nos 2 and 3 is reduced by about 20 per cent compared to single faults oriented in the same manner due to the activations of the main segment. The seismic cycle of the middle (no. 1) fault is also changed. T_s^1 is decreased by an amount of 15 per cent compared to the recurrence time of a single fault (*cf*. Section 4.1), which is a result of the earthquakes occurring on the auxiliary faults.

The behaviour of model B's nos 2 and 3 outer faults is mainly controlled by their orientation in the background stress field. The influence of main-fault earthquakes, whose effect is to lower T_s slightly, is not important compared to the increasing background normal stress, which leads to longer quiet periods between auxiliary fault activations. The side-fault influence on the main segment does not result in a significant change of T_s^1, but in increased magnitudes of the main earthquakes when all segments are activated together.

In general, the fault-zone behaviour depends both on the individual fault orientation in the homogeneous stress field and the mode of interaction between neighbouring segments. The interplay of 'locking' and 'releasing' or triggering effects determines the recurrence-time variations.

4.2.2 Extended leftstep and rightstep geometries

In our final model of a transform fault array, the left- and rightsteps discussed above are further extended along strike (Fig. 9).

The same progressive shear deformation as used in the models above leads to the seismicity pattern displayed in Fig. 10. The plots show the shear zone projected onto the

x-axis against time, where each split-node activation has been marked by a small dot. Since ruptures consist of activations of the whole fault most of the time, these dots generally form simple lines in Fig. 10.

The number of main-fault events during the time span modelled is the same for both models. While model C's auxiliary fault segments (nos 2 and 3) are frequently activated because they are influenced in a triggering sense by faults on both sides, their contribution to the total seismic energy release is quite small ($M_0^{auxil} = 2 \times 10^{19}$ N m compared to $M_0^{main} = 9 \times 10^{19}$ N m). In model D, the shorter faults are oriented with an angle $\beta > 45°$ (which leads to an increasing seismic period with time) and are furthermore subjected to the locking influence of the main faults. As a consequence, they are not activated at all until $t = 200$ yr, but will be shortly afterwards.

Model C shows another effect we consider interesting, the breakdown of the activation symmetry of faults nos 2 and 3. Starting with the event at $t = 64$ yr, the σ_c level at fault 3 reaches its critical level not exactly simultaneously with fault 2. The associated rupture changes the global deformation field and influences the timing and magnitude of further activations on all surrounding faults. The system's performance at the bifurcation point depends on the inhomogeneous stress field in a critical way. Therefore, the behaviour is susceptible to small numerical fluctuations, which are also responsible for the tiny 'precursory' events appearing for $t > 140$ yr, and is thus somewhat undetermined. After the symmetry is broken, imprinted patterns can be traced throughout the activation history and do not change any more. Becker (1997) has studied this phenomenon of fault systems evolving towards an increasingly irregular seismicity in greater detail for fault populations up to 200 cracks.

5 DISCUSSION

We have evaluated the effects of fault orientation and interaction and examined the influence of both mechanisms on the
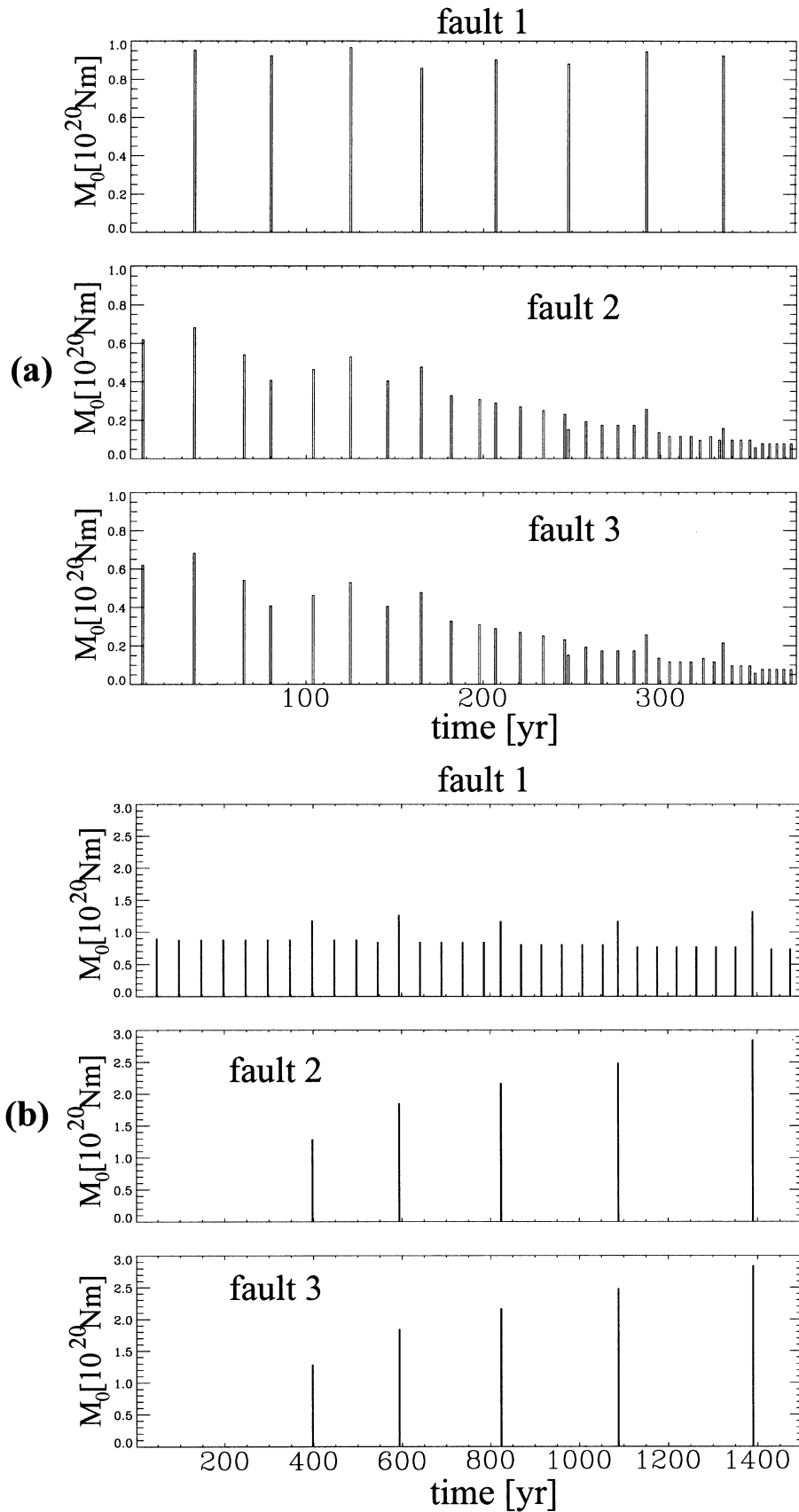
Figure 8. Left- and rightstep seismic moment release. Note the different timescales of models A (a) and B (b).
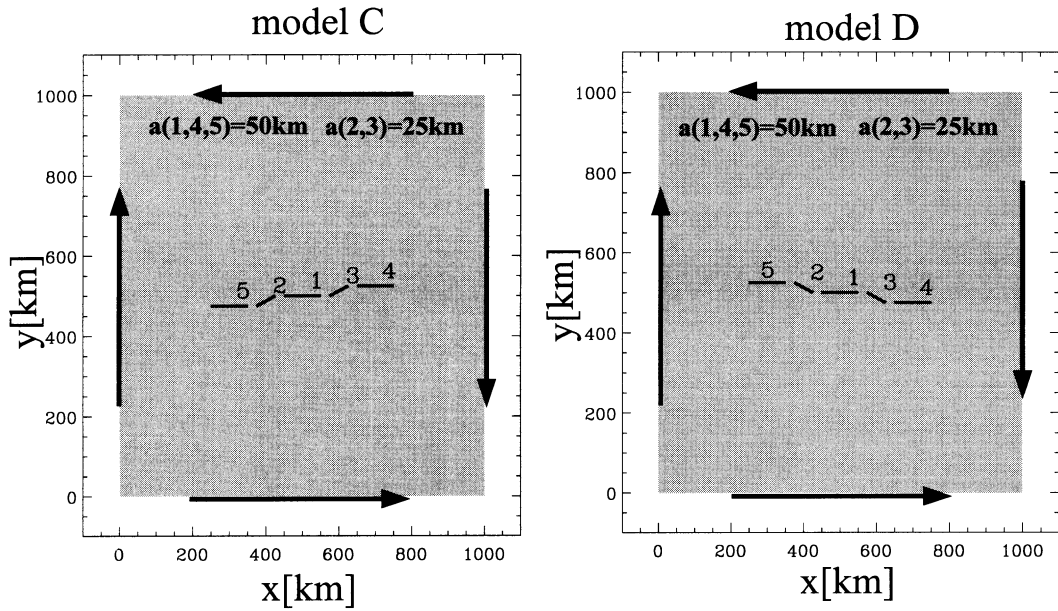
Figure 9. Extended leftstep (model C) and rightstep (model D) geometries.
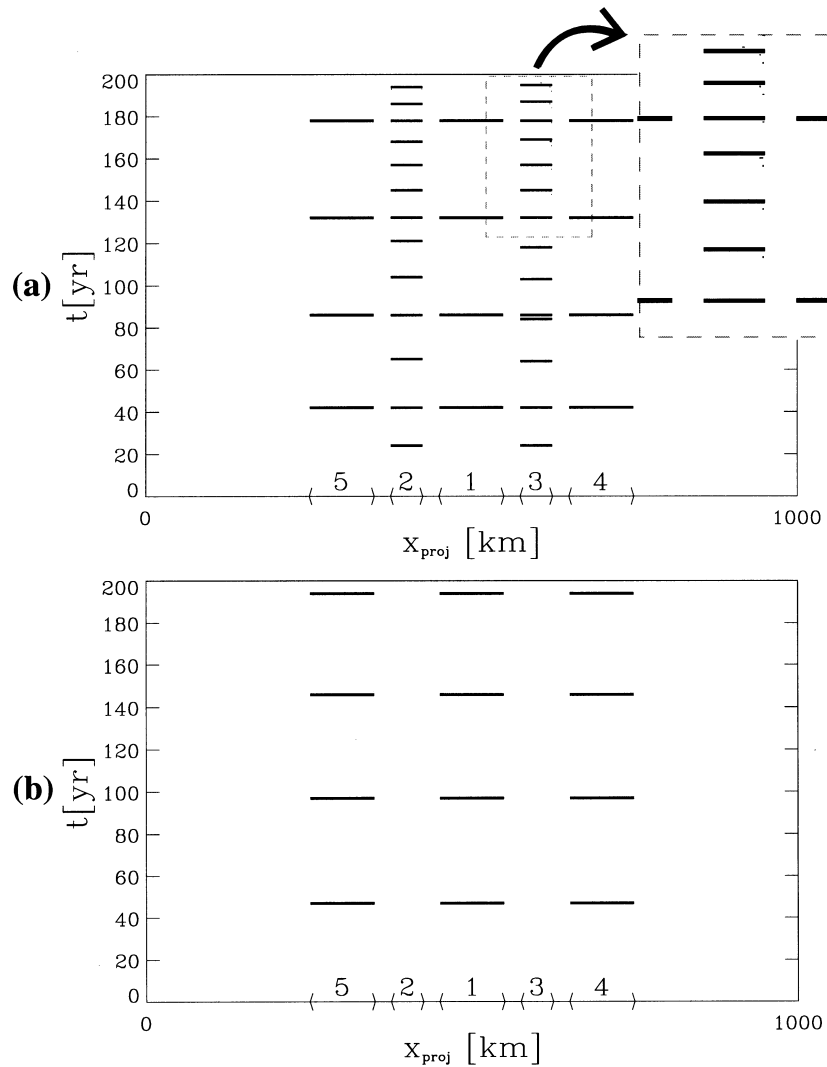
Figure 10. Spatio–temporal seismicity pattern for model C (a) and model D (b). The later deformation stage of fault 3 in model C has been magnified to show small irregularities in the numerical seismicity.

evolution of the seismicity of a fault zone. Single faults may show a varying seismic cycle without any interaction effects, if the fault plane is subjected to different compressional regimes. As indicated by eq. (11) and Fig. 6, the variations of recurrence periods due to changes in σ_n should be detectable if accurate fault event histories are available. Varying cycle characteristics for a single-fault patch could then allow for the inference of what the stress field looked like during the event history and in which way the deformation rates changed. This implies that the simplifications of our model are not too severe. At this time, the available data seem to be too sparse for a global survey examining the relevance of normal-stress field changes at single segments in comparison to interaction effects. Nevertheless, this effect should be kept in mind when examining earthquake sequences and expected recurrence times, even though it might be obscured by the physical mechanisms that we have neglected.

The comparison of single faults and groups of three and five segments in *en echelon* geometries has revealed that interaction can become a relevant factor for groups of faults. Our approach is in some aspects similar to that of Palmer *et al.* (1995). These authors also used split nodes and a static–kinetic friction law to model palaeoseismic earthquake data variations along the San Andreas fault system to examine a main fault with many orthogonally oriented auxiliary faults. Their model showed that the activation of those side faults lead to a modulating effect on the main fault due to local changes of normal stress. As pointed out by Saucier, Humphreys & Weldon 1992, normal stress changes can result in addition from fault-trace-geometry undulations alone.

The direct interaction of faults due to Coulomb stress modification depends on the individual orientations and the relative distances. Although the σ_c stress field can be calculated for arbitrary geometries and media, an order of magnitude estimation is useful. We assume that stress perturbations around a crack are significant when they account for one-tenth of the stress drop. Since the stress field in two dimensions decays with a^2/r^2 in the far field (Pollard & Segall 1987), direct interaction should only be important for relative distances of $O(3a)$ in our model. [The far-field stress field of a double-couple point source in three dimensions decays as r^{-3} (e.g. Lay & Wallace 1995, p. 327). This corresponds to interaction distances of $O(2a)$ when $M_0 \propto a^3$.] However, cascades of triggered events have been observed in systems of larger fault populations (Becker 1997) and might account for long-distance earthquake interactions.

When attempting to interpret our model results for individual activation times and other event data with respect to systems found in nature, the shortcomings of our method have to be discussed. Besides the restriction to plane strain and purely elastic behaviour at crack tips, which has been partly discussed in Section 2.2, one would expect that the detailed behaviour of intersecting faults differs from that of the segments treated here. Connected patches of a shear zone will lead to strong stress concentrations at bends and kinks. These stress fields are expected to be similar to ours with disconnected faults except in the immediate surroundings of the connecting 'bridge'. We expect the stresses to be the same at distances $O(b)$ from the kinks, where b is the dimension of a 'bridge'. The artificial concentration might still be of importance since stress maxima are close to a slipping surface. Hence, a more complete approach should do away with the artificial

restriction of fault-plane extension and take the finite strength of the material into account.

The effect of a viscoelastic substratum not incorporated in our models will be important in two ways. First, during rupture it will exert σ_{xz}, σ_{yz} stresses on the rupturing plate elements, reducing the instantaneous displacement fields and compensating the σ_{xy} stresses. This will result in the same σ_{xy} stress drop with less strike-slip deformation taking place. The static influence of the underlying layers can be estimated by comparing plane-strain results with elastic half-space models. Taking a fault of aspect ratio $2a/W = 0.15$ and a prescribed elliptical slip distribution as an example, the coseismic deformation field resulting from identical maximum displacements (and therefore stress drops) is reduced by about 30 per cent due to the tractions exerted from below compared to the 2-D case.

The second consequence of a viscoelastic layer is that the lithospheric deformation will increase somewhat after each event during the Maxwell time. Since the slip on the fault was smaller than for the fully elastic 2-D problem, shorter recurrence times than those of our models have to be expected. The long-term effects of different viscoelastic models have been studied by Bonafede *et al.* (1986) for infinite strike-slip faults. Their results indicate that under certain boundary conditions the recurrence time is indeed expected to decrease because of the stress relaxation due to past earthquakes.

In our models, the steady increase of shear stress on 'locked' segments yields growing magnitudes and stress drops for subsequent events. This effect may be of only limited importance in nature. Since the surrounding stress field around these segments reaches very high values, one would expect the activation, or even the creation, of new secondary faults with a more suitable β orientation. However, our basic findings regarding the recurrence time as a function of orientation angle β and the mode of interaction are not affected.

We note that in our models, simultaneous multisegment events always lead to the same stress drops in two classes of faults (e.g. faults 1, 4 & 5 and faults 2 & 3 of Figs 9 and 10). Although mechanical interaction between the faults is accounted for during the iteration process of stress drop at active fault segments, the dynamics of rupture propagation and elastic-wave radiation may lead to more complex patterns of interaction and thus different stress drops. This in turn might break the symmetry at an earlier stage. Ruff (1996) has suggested that varying stress drops on interacting fault segments may lead to irregular recurrence times.

6 CONCLUSIONS

We have shown that the earthquake recurrence time found at isolated fault segments depends on their orientations with respect to the regional shear stress, termed β, when they are subjected to a progressive shear deformation field. The seismic cycle can only be expected to remain perfectly periodic with progressing time for the special case of $\beta = 45°$. A different value for β will result in recurrence-time variations even if the frictional constants are assumed to be constant in time. If changing trends are found in seismic data sets, a normal stress change with respect to the recent segment orientation might be inferred. A more important implication is maybe that this result should be taken into account when the underlying concepts of the seismic cycle leading to the proposed time- and slip-predictable models are considered. Constant frictional

parameters, strain rate and fault-zone configurations will only under certain circumstances lead to a constant seismic cycle.

The evolution of seismicity patterns in multifault systems is influenced by a second effect, the mode of interaction due to Coulomb stress modification. The importance of each mechanism and the dependence on relative distances as well as orientations were examined for various examples. Fault interaction might be one of the major reasons that studies seeking to demonstrate the validity of earthquake recurrence models have failed.

Our results suggest that regular seismic cycles will not be the rule but the exception at fault segments found in nature. If regular activations are found, this may be a result of the recruitment of new fault segments that are more efficiently oriented in the local stress field.

REFERENCES

Bakun, W. & McEvilly, T., 1984. Recurrence models and Parkfield, California earthquakes, *J. geophys. Res.,* **89,** 3051–3058.

Becker, T.W., 1997. Finite element modeling of fault zone interactions, *Diploma thesis,* Institut für Meteorologie und Geophysik der J.W. Goethe-Universität, Frankfurt am Main, (in German).

Bonafede, M., Dragoni, M. & Boschi, E., 1985. Quasi-static crack models and the frictional stress threshold criterion for slip arrest, *J. geophys. Res.,* **83,** 615–637.

Bonafede, M., Dragoni, M. & Morelli, A., 1986. On the existence of a periodic dislocation cycle in horizontally layered viscoelastic models, *J. geophys. Res.,* **91,** 9396–6404.

Burridge, R. & Halliday, G., 1971. Dynamic shear cracks with friction as models for shallow focus earthquakes, *Geophys. J. R. astr. Soc.,* **25,** 261–283.

Byerlee, J., 1978. Friction of rock, *Pure appl. Geophys.,* **116,** 615–626.

Calpin, J.P., 1996. *Paleoseismology,* Academic Press, New York.

Chen, K., Bak, P. & Obukhov, S.P., 1991. Self-organized criticality in a crack-propagation model of earthquakes, *Phys. Rev.* A, **43,** 625–629.

Chinnery, M.A., 1963. The stress changes that accompany strike-slip faulting, *Bull. seism. Soc. Am.,* **53,** 921–932.

Dahm, T. & Becker, T., 1998. On the elastic properties of media containing strongly interacting in-plane cracks, *Pure appl. Geophys.,* **151,** 1–16.

DeMets, C., Gordon, R.G., Argus, D.F. & Stein, S., 1990. Current plate motions, *Geophys. J. Int.,* **101,** 425–478.

Deng, J. & Sykes, L.R., 1997. Evolution of the stress field in Southern California and triggering of moderate-size earthquakes: a 200-year perspective, *J. geophys. Res.,* **102,** 9859–9886.

Goes, S.D.B., 1996. Irregular recurrence of large earthquakes: an analysis of historic and paleoseismic catalogs, *J. geophys. Res.,* **101,** 5739–5749.

Harris, R.A., Simpson, R.W. & Reasenberg, P.A., 1995. Influence of static stress changes on earthquake locations in Southern California, *Nature,* **375,** 221–224.

Heimpel, M. & Olson, P., 1996. A seismodynamical model of lithosphere deformation: development of continental and oceanic rift networks, *J. geophys. Res.,* **101,** 16 155–16 176.

Hudnut, K.W., Seeber, L. & Pacheco, J., 1989. Cross-fault triggering in the November 1987 Superstition Hills Earthquake sequence, Southern California, *Geophys. Res. Lett.,* **16,** 199–202.

King, G., Stein, R.C. & Lin, J., 1994. Static stress change and the triggering of earthquakes, *Bull. seism. Soc. Am.,* **84,** 935–953.

Lachenbruch, A.H. & Sass, J.H., 1980. Heat flow and energetics of the San Andreas fault zone, *J. geophys. Res.,* **85,** 6185–6222.

Lay, T. & Wallace, T., 1995. *Modern Global Seismology,* Academic Press, San Diego.

Li, V.C. & Rice, J., 1987. Crustal deformation in great California earthquake cycles, *J. geophys. Res.,* **92,** 11 533–11 551.

Lyzenga, G.A., Raefsky, A. & Mulligan, S.G., 1991. Models of recurrent strike-slip earthquake cycles and the state of crustal stress, *J. geophys. Res.,* **96,** 21 623–21 640.

Marone, C., 1998. Laboratory-derived friction laws and their application to seismic faulting, *Ann. Rev. Earth planet. Sci.,* **26,** in press.

Marone, C., Vidale, J.E. & Ellsworth, W., 1995. Fault healing inferred from the time dependent variations in source properties of repeating earthquakes, *Geophys. Res. Lett.,* **22,** 3095–3098.

Melosh, H. & Raefsky, A., 1981. A simple and efficient method for introducing faults into finite element computations, *Bull. seism. Soc. Am.,* **71,** 1391–1400.

Mulargia, F. & Gasperini, P., 1995. Evaluation of the applicability of the time- and slip-predictable earthquake recurrence models to Italian seismicity, *Geophys. J. Int.,* **120,** 453–473.

Nishenko, S.P. & Buland, R., 1987. A generic recurrence interval distribution for earthquake forecasting, *Bull. seism. Soc. Am.,* **77,** 1382–1389.

Nur, A. & Booker, J., 1972. Aftershocks caused by pore fluid flow?, *Science,* **175,** 885–887.

Okada, Y., 1992. Internal deformation due to shear and tensile faults in a half-space, *Bull. seism. Soc. Am.,* **82,** 1018–1040.

Palmer, R., Weldon, R., Humphrey, E. & Saucier, F., 1995. Earthquake recurrence on the southern San Andreas modulated by fault-normal stress, *Geophys. Res. Lett.,* **22,** 535–538.

Pollard, D.D. & Segall, P., 1987. Theoretical displacements and stresses near fractures in rock: with applications to faults, joints, veins, dikes, and solution surfaces, in *Fracture Mechanics of Rock,* pp. 277–350, ed. Atkinson, B.K., Academic Press, London.

Purcaru, G. & Berckhemer, H., 1978. A magnitude scale for very large earthquakes, *Tectonophysics,* **49,** 189–198.

Reasenberg, P.A. & Simpson, R.W., 1992. Response of regional seismicity to the static stress change produced by the Loma Prieta earthquake, *Science,* **255,** 1687–1690.

Reid, H.F., 1910. The mechanics of the earthquake, in *The California Earthquake of April 18, 1906,* Rep. State Invest. Comm., Vol. 2, pp. 16–28, Carnegie Institution, Washington, DC.

Rice, J.R. & Tse, S.T., 1986. Dynamic motion of a single degree of freedom system following a rate and state dependent friction law, *J. geophys. Res.,* **91,** 521–530.

Ruff, L.J., 1996. Large earthquakes in subduction zones: segment interaction and recurrence times, in *Subduction: Top to Bottom,* eds Bebout, G.E., Scholl, D.W., Kirby, S.H. & Platt, J.P., *Am. Geophys. Un. Monogr.,* **96,** 91–104.

Rundle, J., 1988a. A physical model for earthquakes. 1. Fluctuations and interactions, *J. geophys. Res.,* **93,** 6237–6254.

Rundle, J., 1988b. A physical model for earthquakes. 2. Applications to Southern California, *J. geophys. Res.,* **93,** 6255–6274.

Saucier, F., Humphreys, E. & Weldon, R.I., 1992. Stress near geometrically complex strike-slip faults: application to the San Andreas fault at Cajon pass, Southern California, *J. geophys. Res.,* **97,** 5081–5094.

Schmittbuhl, J., Vilotte, J.-P. & Roux, S., 1996. Velocity weakening friction: a renormalization approach, *J. geophys. Res.,* **101,** 13 911–13 917.

Scholz, C.H., 1974. Post-earthquake dilatancy recovery, *Geology, 2,* 551–554.

Scholz, C.H., 1990. *The Mechanics of Earthquakes and Faulting,* Cambridge University Press, Cambridge.

Segall, P. & Pollard, D., 1980. Mechnanics of discontinuous faults, *J. geophys. Res., 85,* 4337–4350.

Shewchuk, J.R., 1996. Triangle: engineering a 2D quality mesh generator and delaunay triangulator, in *First Workshop on Applied Computational Geometry,* pp. 124–133, Association for Computing Machinery, Philadelphia, PA.

Shimazaki, K. & Nakata, T., 1980. Time-predictable recurrence model for large earthquakes, *Geophys. Res. Lett., 7,* 279–282.

Sieh, K., Stuiver, M. & Brillinger, D., 1989. A more precise chronology of earthquakes produced by the San Andreas fault in Southern California, *J. geophys. Res., 94,* 603–623.

Stein, R.S. & Lisowski, M., 1983. The 1979 Homestead Valley earthquake sequence, California: control of aftershocks and postseismic deformation, *J. geophys. Res., 88,* 6477–6490.

Stuart, W.D., 1986. Forecast model for large and great earthquakes in Southern California, *J. geophys. Res., 91,* 13 771–13 786.

Sykes, L.R. & Quittmeyer, R.C., 1981. Repeat times of great earthquakes on simple plate boundaries, in *Third Maurice Ewing Symposium on Earthquake Predictions,* Vol. 4, pp. 217–247, eds Simpson, D.W. & Richards, P., AGU, Washington, DC.

Ward, S.N., 1996. A synthetic seismicity model for Southern California: cycles, probabilities, and hazard, *J. geophys. Res., 101,* 22 393–22 418.

Zienkiewicz, O., 1977. *The Finite Element Method,* 3rd edn, McGraw-Hill, London.